ABSTRACT

RNTUPLE FOR ATLAS ANALYSIS WORKFLOWS

Fatima Rodriguez, M.A.
Department of Physics
Northern Illinois University, 2025
Hector de la Torre, Director

RNTuple is the new data storage format set to replace TTree at the start of the High Luminosity LHC. An investigation was conducted on how analysis workflows for ATLAS researchers will change with RNTuple. Additionally, performance studies have been conducted that demonstrate an improvement in speed and memory usage at the analysis front. Finally, different compression algorithms were tested and it was found that blah blah remains to best work with RNTuple.

NORTHERN ILLINOIS UNIVERSITY
DE KALB, ILLINOIS

DECEMBER 2025

RNTUPLE FOR ATLAS ANALYSIS WORKFLOWS

BY

FATIMA RODRIGUEZ

A DISSERTATION SUBMITTED TO THE GRADUATE SCHOOL

IN PARTIAL FULFILLMENT OF THE REQUIREMENTS

FOR THE DEGREE

MASTER OF PHYSICS

DEPARTMENT OF PHYSICS

Dissertation Director:
Hector de la Torre

ACKNOWLEDGEMENTS

Thanks thanks

DEDICATION

Thanks thanks

TABLE OF CONTENTS

Page

LIST OF FIGURES

CHAPTER 1

INTRODUCTION

Our current understanding of the building blocks of our universe is summarized with one model, called the Standard Model (SM) [4]. From the way we power our cities, to the particles that hold them together, the SM explains how the basic building blocks of matter interact, governed by fundamental forces: electromagnetism, the strong force and the weak force. Yet, questions remain about the SM, such as is there a unification theory that includes gravity? Why are there only three generations of fundamental particles? What is the nature of dark matter and dark energy, and how does it fit within the SM? What about the origin of the matter-antimatter asymmetry? Is the SM complete or do other exotic particles exists? Over the years, experimental particle physicists and engineers have built technology to test the SM, either by performing precision measurements of particles and their behaviors, or by colliding particles and measuring their outputs. As a result, we have increased our confidence in the SM theory, but continue to search for answers for these remaining questions through experimental discovery.

A Toroidal LHC Apparatus (ATLAS) [2] is a particle physics experiment designed to detect the high-energy particle collisions from the Large Hadron Collider (LHC) [29]. [FATIMA NEEDS TO FIX THIS PARAGRAPH]At the LHC, collisions take place at a rate of more than a billion interactions per second, which is a combined data volume of about 60 million megabytes per second . In order to study rare processes, the LHC will have a major upgrade to increase the number of collisions by a factor of 5 to 7.5. This upgrade, called the High-Luminosity LHC (HL-LHC), will require a new data storage format that can handle this increase in data.

RNTuple [32] is the new ROOT [27] data storage format that will be in use at the start of the HL-LHC [24]. RNTuple takes advantage of modern C++ techniques, which have shown to improve read speedability and memory usage when compared to its predecessor, TTree, and other data storage formats such as HDF5 and Parquet [28]. At the start of this work, performance studies on RNTuple were conducted at the production level, and RNTuple was still at an experimental stage.

This thesis investigates the performance of RNTuple for ATLAS analysis workflows. This chapter will provide a more detailed introduction of the SM, followed by an introduction to the ATLAS experiment and its detector technology in Chapter 2. In Chapter 3, the ATLAS software and computing system, and data contents are introduced. In Chapter 4, an introduction to RNTuple and TTree is provided along with examples of how RNTuple is applied in comparison to TTree. Performance studies conducted for RNTuple and how they compare with TTree will be presented in Chapter 5. In Chapter 6, the Analysis Grand Challenge (AGC) is introduced along with its RNTuple implementation. A final discussion and conclusions are given in Chapter 7.

1.1 Standard Model of Particle Physics

The SM is a quantum field theory that explains and catagorizes all observed fundamental particles by their properties and interactions. Quantum field theory (QFT) is the main theoretical tool for describing particle interactions by combining special relativity and quantum mechanics. Due to this combination, QFT is a probabilistic theory where each particle has an associated field that permeates all of space; therefore, forces are simply the interactions between these different fields. For example, the electromagnetic force is just the interaction between the electromagnetic field and charged matter fields, which fall under quantum electrodynamics (QED). In sum, the SM encompasses all known elementary particle interactions, except for gravity, through a collection of quantum field theories, and each are dictated by gauge symmetries: QED ($U(1)$), the Glashow-Weinberg-Salam theory of electroweak processes ($SU(3)$), and quantum chromodynamics ($SU(2) \times U(1)$).

The four groups of particles shown in Figure 1.1: quarks, leptons, gauge bosons, and scalar bosons, can be further categorized as *bosons* or *fermions* because of a fundamental property called spin. Similar to the Earth, particles carry orbital angular momentum and spin angular momentum; however, for particles, spin is an intrinsic property. All bosons carry an integer spin; while, fermions carry half-integer spin. As a result from QFT, each fermion has an antiparticle with the same mass and lifetime as the particle itself, but oppositely charged. The three charged leptons (e, μ, τ) are massive, while their corresponding nuetrinos (ν_e,ν_μ,ν_τ), are massless with nuetral charge. Due to QCD, there are 8 types of gluons. The Higgs boson has its own section as a scalar boson because unlike the vector bosons with spin 1, the Higgs boson has spin 0. In sum, there are a total of 12 leptons including their antiparticles, 36 quarks including all the flavors and their antiparticles, 12 vector bosons, and 1 scalar boson, which makes a total of 61 fundamental particles.

1.2 Phenomenology of Large Hadron Colliders

Symmetries found in the SM are followed by conservation laws through Noether's Theorem, which can be experimentally verified. Collider experiments serve as probes to the SM because they directly test those conservation laws through the detection of final state radiation. To produce elementary particles, the energy in the center of mass frame must be greater than the sum of masses of the produced particles. In other words, increasing the center of mass energy increases the available phase space for new particle production.

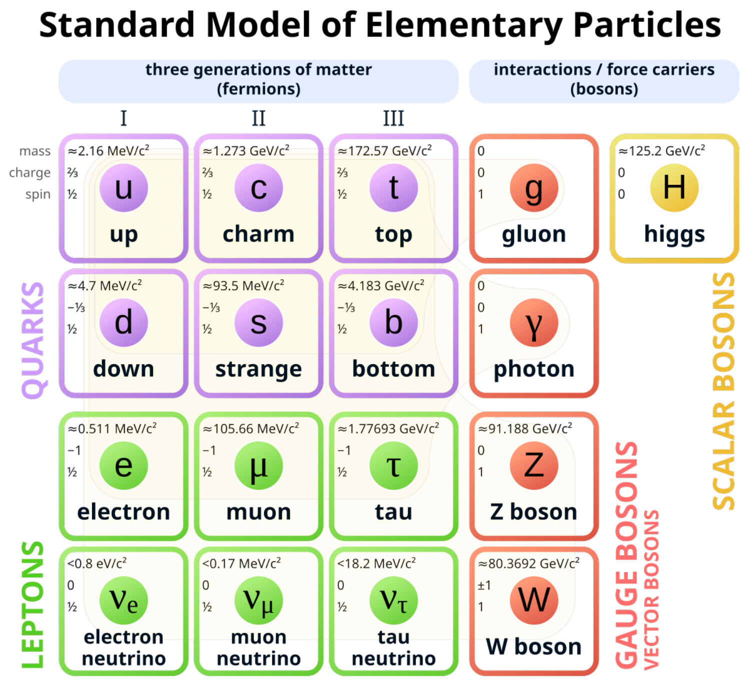

Figure 1.1: Particle content of the Standard Model [?].

The center of mass energy of a particle collision is calculated by taking the square root of the Lorentz invariant, as shown in Equation 1.1, where E_i and p_i are the total energy and momentum of the two initial particle states.

$$\sqrt{s} = \sqrt{(\sum_{i=1}^{2} E_i)^2 - (\sum_{i=1}^{2} p_i)^2} \tag{1.1}$$

In colliders, two beams of particles are accelerated to reach high energies and brought together for collision. Each collision is called an event and specific interactions or transformations are called processes. Through QFT, the rate of a process, called cross-sections, can be predicted via the particle kinematics, their properties, and the properties of the process. Experimentally, cross-sections can be calculated via Equation 1.2, where N is the number

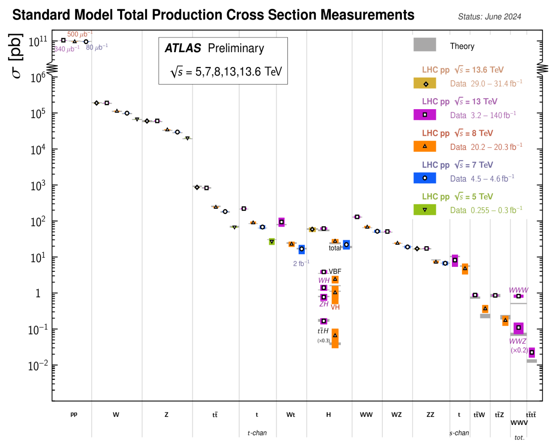

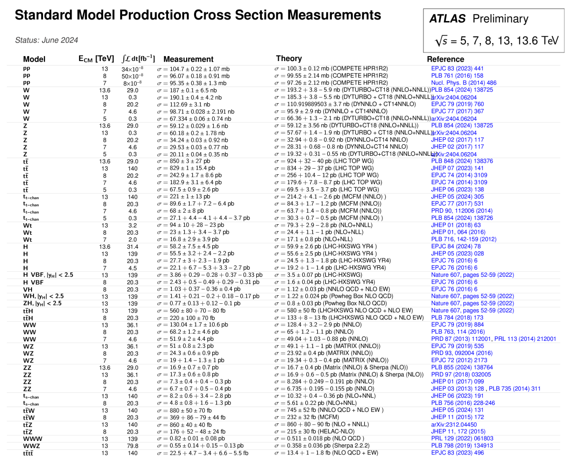

Model	E_{CM} [TeV]	$\int\mathcal{L}\,dt$[fb^{-1}]	Measurement	Theory	Reference
pp	13	34×10^{-8}	$\sigma = 104.7 \pm 0.22 \pm 1.07$ mb	$\sigma = 100.3 \pm 0.12$ mb (COMPETE HPR1R2)	EPJC 83 (2023) 441
pp	8	50×10^{-8}	$\sigma = 96.07 \pm 0.18 \pm 0.91$ mb	$\sigma = 99.55 \pm 2.14$ mb (COMPETE HPR1R2)	PLB 761 (2016) 158
pp	7	8×10^{-8}	$\sigma = 95.35 \pm 0.38 \pm 1.3$ mb	$\sigma = 97.26 \pm 2.12$ mb (COMPETE HPR1R2)	Nucl. Phys. B (2014) 486
W	13.6	29.0	$\sigma = 187 \pm 0.1 \pm 6.5$ nb	$\sigma = 193.2 + 3.8 - 5.9$ nb (DYTURBO+CT18 (NNLO+NNLL))	PLB 854 (2024) 138725
W	13	0.3	$\sigma = 190.1 \pm 0.4 \pm 4.2$ nb	$\sigma = 185.3 + 3.8 - 5.5$ nb (DYTURBO + CT18 (NNLO+NNLL))	arXiv:2404.06204
W	8	20.2	$\sigma = 112.69 \pm 3.1$ nb	$\sigma = 110.919889503 \pm 3.7$ nb (DYNNLO + CT14NNLO)	EPJC 79 (2019) 760
W	7	4.6	$\sigma = 98.71 \pm 0.028 \pm 2.191$ nb	$\sigma = 95.9 \pm 2.9$ nb (DYNNLO + CT14NNLO)	EPJC 77 (2017) 367
W	5	0.3	$\sigma = 67.334 \pm 0.06 \pm 0.74$ nb	$\sigma = 66.36 + 1.3 - 2.1$ nb (DYTURBO+CT18 (NNLO+NNLL))	arXiv:2404.06204
Z	13.6	29.0	$\sigma = 59.12 \pm 0.029 \pm 1.6$ nb	$\sigma = 59.12 \pm 3.56$ nb (DYTURBO+CT18 (NNLO+NNLL))	PLB 854 (2024) 138725
Z	13	0.3	$\sigma = 60.18 \pm 0.2 \pm 1.78$ nb	$\sigma = 57.67 + 1.4 - 1.9$ nb (DYTURBO + CT18 (NNLO+NNLL))	arXiv:2404.06204
Z	8	20.2	$\sigma = 34.24 \pm 0.03 \pm 0.92$ nb	$\sigma = 32.94 + 0.8 - 0.92$ nb (DYNNLO+CT14 NNLO)	JHEP 02 (2017) 117
Z	7	4.6	$\sigma = 29.53 \pm 0.03 \pm 0.77$ nb	$\sigma = 28.31 + 0.68 - 0.8$ nb (DYNNLO+CT14 NNLO)	JHEP 02 (2017) 117
Z	5	0.3	$\sigma = 20.11 \pm 0.04 \pm 0.35$ nb	$\sigma = 19.32 + 0.31 - 0.55$ nb (DYTURBO+CT18 (NNLO+NNLL))	arXiv:2404.06204
$t\bar{t}$	13.6	29.0	$\sigma = 850 \pm 3 \pm 27$ pb	$\sigma = 924 + 32 - 40$ pb (LHC TOP WG)	PLB 848 (2024) 138376
$t\bar{t}$	13	140	$\sigma = 829 \pm 1 \pm 15.4$ pb	$\sigma = 834 + 29 - 37$ pb (LHC TOP WG)	JHEP 07 (2023) 141
$t\bar{t}$	8	20.2	$\sigma = 242.9 \pm 1.7 \pm 8.6$ pb	$\sigma = 256 + 10.4 - 12$ pb (LHC TOP WG)	EPJC 74 (2014) 3109
$t\bar{t}$	7	4.6	$\sigma = 182.9 \pm 3.1 \pm 6.4$ pb	$\sigma = 179.6 + 7.8 - 8.7$ pb (LHC TOP WG)	EPJC 74 (2014) 3109
$t\bar{t}$	5	0.3	$\sigma = 67.5 \pm 0.9 \pm 2.6$ pb	$\sigma = 69.5 + 3.5 - 3.7$ pb (LHC TOP WG)	JHEP 06 (2023) 138
t_{t-chan}	13	140	$\sigma = 221 \pm 1 \pm 13$ pb	$\sigma = 214.2 + 4.1 - 2.6$ pb (MCFM (NNLO))	JHEP 05 (2024) 305
t_{t-chan}	8	20.3	$\sigma = 89.6 \pm 1.7 + 7.2 - 6.4$ pb	$\sigma = 84.3 + 1.7 - 1.2$ pb (MCFM (NNLO))	EPJC 77 (2017) 531
t_{t-chan}	7	4.6	$\sigma = 68 \pm 2 \pm 8$ pb	$\sigma = 63.7 + 1.4 - 0.8$ pb (MCFM (NNLO))	PRD 90, 112006 (2014)
t_{t-chan}	5	0.3	$\sigma = 27.1 + 4.4 - 4.1 + 4.4 - 3.7$ pb	$\sigma = 30.3 + 0.7 - 0.5$ pb (MCFM (NNLO))	PLB 854 (2024) 138726
Wt	13	3.2	$\sigma = 94 \pm 10 + 28 - 23$ pb	$\sigma = 79.3 + 2.9 - 2.8$ pb (NLO+NNLL)	JHEP 01 (2018) 63
Wt	8	20.3	$\sigma = 23 \pm 1.3 + 3.4 - 3.7$ pb	$\sigma = 24.4 + 1.1 - 1$ pb (NLO+NLL)	JHEP 01, 064 (2016)
Wt	7	2.0	$\sigma = 16.8 \pm 2.9 \pm 3.9$ pb	$\sigma = 17.1 \pm 0.8$ pb (NLO+NLL)	PLB 716, 142-159 (2012)
H	13.6	31.4	$\sigma = 58.2 \pm 7.5 \pm 4.5$ pb	$\sigma = 59.9 \pm 2.6$ pb (LHC-HXSWG YR4)	EPJC 84 (2024) 78
H	13	139	$\sigma = 55.5 \pm 3.2 + 2.4 - 2.2$ pb	$\sigma = 55.6 \pm 2.5$ pb (LHC-HXSWG YR4)	JHEP 05 (2023) 028
H	8	20.3	$\sigma = 27.7 \pm 3 + 2.3 - 1.9$ pb	$\sigma = 24.5 + 1.3 - 1.8$ pb (LHC-HXSWG YR4)	EPJC 76 (2016) 6
H	7	4.5	$\sigma = 22.1 + 6.7 - 5.3 + 3.3 - 2.7$ pb	$\sigma = 19.2 + 1 - 1.4$ pb (LHC-HXSWG YR4)	EPJC 76 (2016) 6
H VBF, $\lvert y_H\rvert < 2.5$	13	139	$\sigma = 3.86 + 0.29 - 0.28 + 0.37 - 0.33$ pb	$\sigma = 3.5 \pm 0.07$ pb (LHC-HXSWG)	Nature 607, pages 52-59 (2022)
H VBF	8	20.3	$\sigma = 2.43 + 0.5 - 0.49 + 0.29 - 0.31$ pb	$\sigma = 1.6 \pm 0.04$ pb (LHC-HXSWG YR4)	EPJC 76 (2016) 6
VH	8	20.3	$\sigma = 1.03 + 0.37 - 0.36 \pm 0.4$ pb	$\sigma = 1.12 \pm 0.03$ pb (NNLO QCD + NLO EW)	EPJC 76 (2016) 6
WH, $\lvert y_H\rvert < 2.5$	13	139	$\sigma = 1.41 + 0.21 - 0.2 + 0.18 - 0.17$ pb	$\sigma = 1.22 \pm 0.024$ pb (Powheg Box NLO QCD)	Nature 607, pages 52-59 (2022)
ZH, $\lvert y_H\rvert < 2.5$	13	139	$\sigma = 0.77 \pm 0.13 + 0.12 - 0.1$ pb	$\sigma = 0.8 \pm 0.03$ pb (Powheg Box NLO QCD)	Nature 607, pages 52-59 (2022)
$t\bar{t}H$	13	139	$\sigma = 560 \pm 80 + 70 - 80$ fb	$\sigma = 580 \pm 50$ fb (LHCHXSWG NLO QCD + NLO EW)	Nature 607, pages 52-59 (2022)
$t\bar{t}H$	8	20.3	$\sigma = 220 \pm 100 \pm 70$ fb	$\sigma = 133 + 8 - 13$ fb (LHCHXSWG NLO QCD + NLO EW)	PLB 784 (2018) 173
WW	13	36.1	$\sigma = 130.04 \pm 1.7 \pm 10.6$ pb	$\sigma = 128.4 + 3.2 - 2.9$ pb (NNLO)	EPJC 79 (2019) 884
WW	8	20.3	$\sigma = 68.2 \pm 1.2 \pm 4.6$ pb	$\sigma = 65 + 1.2 - 1.1$ pb (NNLO)	PLB 763, 114 (2016)
WW	7	4.6	$\sigma = 51.9 \pm 2 \pm 4.4$ pb	$\sigma = 49.04 + 1.03 - 0.88$ pb (NNLO)	PRD 87 (2013) 112001, PRL 113 (2014) 212001
WZ	13	36.1	$\sigma = 51 \pm 0.8 \pm 2.3$ pb	$\sigma = 49.1 + 1.1 - 1$ pb (MATRIX (NNLO))	EPJC 79 (2019) 535
WZ	8	20.3	$\sigma = 24.3 \pm 0.6 \pm 0.9$ pb	$\sigma = 23.92 \pm 0.4$ pb (MATRIX (NNLO))	PRD 93, 092004 (2016)
WZ	7	4.6	$\sigma = 19 + 1.4 - 1.3 \pm 1$ pb	$\sigma = 19.34 + 0.3 - 0.4$ pb (MATRIX (NNLO))	EPJC 72 (2012) 2173
ZZ	13.6	29.0	$\sigma = 16.9 \pm 0.7 \pm 0.7$ pb	$\sigma = 16.7 \pm 0.4$ pb (Matrix (NNLO) & Sherpa (NLO))	PLB 855 (2024) 138764
ZZ	13	36.1	$\sigma = 17.3 \pm 0.6 \pm 0.8$ pb	$\sigma = 16.9 + 0.6 - 0.5$ pb (Matrix (NNLO) & Sherpa (NLO))	PRD 97 (2018) 032005
ZZ	8	20.3	$\sigma = 7.3 \pm 0.4 + 0.4 - 0.3$ pb	$\sigma = 8.284 + 0.249 - 0.191$ pb (NNLO)	JHEP 01 (2017) 099
ZZ	7	4.6	$\sigma = 6.7 \pm 0.7 + 0.5 - 0.4$ pb	$\sigma = 6.735 + 0.195 - 0.155$ pb (NNLO)	JHEP 03 (2013) 128 , PLB 735 (2014) 311
t_{s-chan}	13	140	$\sigma = 8.2 \pm 0.6 + 3.4 - 2.8$ pb	$\sigma = 10.32 + 0.4 - 0.36$ pb (NLO+NNL)	JHEP 06 (2023) 191
t_{s-chan}	8	20.3	$\sigma = 4.8 \pm 0.8 + 1.6 - 1.3$ pb	$\sigma = 5.61 \pm 0.22$ pb (NLO+NNL)	PLB 756 (2016) 228-246
$t\bar{t}W$	13	140	$\sigma = 880 \pm 50 \pm 70$ fb	$\sigma = 745 \pm 52$ fb (NNLO QCD + NLO EW)	JHEP 05 (2024) 131
$t\bar{t}W$	8	20.3	$\sigma = 369 + 86 - 79 \pm 44$ fb	$\sigma = 232 \pm 32$ fb (MCFM)	JHEP 11 (2015) 172
$t\bar{t}Z$	13	140	$\sigma = 860 \pm 40 \pm 40$ fb	$\sigma = 860 + 80 - 90$ fb (NLO + NNLL)	arXiv:2312.04450
$t\bar{t}Z$	8	20.3	$\sigma = 176 + 52 - 48 \pm 24$ fb	$\sigma = 215 \pm 30$ fb (HELAC-NLO)	JHEP 11, 172 (2015)
WWW	13	139	$\sigma = 0.82 \pm 0.01 \pm 0.08$ pb	$\sigma = 0.511 \pm 0.018$ pb (NLO QCD)	PRL 129 (2022) 061803
WWZ	13	79.8	$\sigma = 0.55 \pm 0.14 + 0.15 - 0.13$ pb	$\sigma = 0.358 \pm 0.036$ pb (Sherpa 2.2.2)	PLB 798 (2019) 134913
$t\bar{t}t\bar{t}$	13	140	$\sigma = 22.5 + 4.7 - 3.4 + 6.6 - 5.5$ fb	$\sigma = 13.4 + 1 - 1.8$ fb (NLO QCD + EW)	EPJC 83 (2023) 496

Figure 1.2: Summary of several Standard Model cross-section measurements (a) with associated references (b) [1]. Processes with smaller cross-sections are considered rare-processes because it has a lower probability of being observed. Increasing the probability of these rare-processes would require an increase of energy. The measurements are corrected for branching fractions, compared to the corresponding theoretical expectations.

of events for the process being measured and L is the instantaneous luminosity, defined in Equation as 1.3.

$$\sigma = \frac{N}{\int Ldt} \tag{1.2}$$

$$L = f\frac{n_1 n_2}{4\pi\sigma_x\sigma_y} \tag{1.3}$$

f is the frequency of collisions, n_1 and n_2 are the number of particles in the colliding bunches. σ_x and σ_y are the root-mean-squared horizontal and vertical beam sizes. Figure 1.2 displays the predicted cross-sections for certain processes and the required center of mass energies for those processes to be observed.

The produced particles are detected and verified by conservation laws. When high-energy charged particles pass through matter, they ionize atoms along their path. Ions then serve as "seeds" for cloud chambers or sparks for sparks chambers. Their classification is then calculated by the energy differences detected from those "seeds. Neutral particles are not detected but reconstructed by calculating the conservation of momuentum of a particular process.

CHAPTER 2

THE ATLAS EXPERIMENT

In October 1992, the ATLAS collaboration, submited a letter of intent to the LHC Experiment Committee highlighting the design of what came to be today's ATLAS Experiment [2]. From the start, ATLAS was designed to be a general-purpose experiment, optimized to search for the Higgs boson, top quark decays, and supersymmetry. In July 1997, the ATLAS Experiment was approved and by November 2008, ATLAS was the largest detector ever constructed at 44 meters long and 25 meters in diameter. By November 2009, ATLAS recorded its first proton-proton collision and by December 2010, ATLAS was first to observed the production of top quark pairs, which are the heaviest known elementary particle with a strong coupling to the Higgs boson. By July 2012, both ATLAS and the Compact Muon Spectrometer (CMS) experiment successfully observed the Higgs boson [12, 13]. ATLAS is projected to continue operation until 2035 to continue searching for standing questions from the SM. This chapter will serve as an introduction to the LHC and the ATLAS detector.

2.1 The Large Hadron Collider

The LHC is a two-ring-superconducting-hadron accelerator and collider built outside of Geneva, Switzerland at the Conseil Europeen pour la Recherche Nucleaire (CERN) [29]. It was approved for construction in 1996 to search for beyond the SM physics at energies larger than 10 TeV. It's approval was heavily influenced by the cost-saving idea of reusing the existing 26.5 km tunnels from the Large Electron-Positron (LEP) collider [14]. The LHC has four main collision points that house the ATLAS, CMS, Large Hadron Collider beauty (LHCb), and A Large Ion Collider Experiment (ALICE). ATLAS and CMS are the two high-energy experiments located at diametrically opposite straight sections. LHCb is a low luminosity experiment dedicated to investigate the difference between matter and anti-matter by detecting b quarks. ALICE is an ion experiment dedicated to studying quark-gluon plasma forms.

The LHC is initially supplied with protons from the injector complex, which is a sequence of accelerators. The process begins with hydrogen gas stored an insulation vacuum that then enters the Linear accelerator 4 (Linac4). Linac4 is designed to boost negative hydrogen ions to 160 MeV. Those ions then enter the Proton Synchrotron Booster, which is made up for four superimposed synchroton rings. During injection, the ions are stripped of their two electrons, leaving only protons. Those protons are then accelerated to 2 GeV into the Proton Synchrotron (PS). In PS, the protons increase their energy to 25 GeV. Then they enter the Super Proton Synchrotron (SPS) to further accelerate up to 450 GeV. The protons get injected into the LHC main ring, where their final acceleration to 7 TeV occurs. A full picture of the accelerator complex is found in Figure 2.1.

The three main components within each of these accelerators are magnets, vacuum chambers, and radiofrequency (RF) cavities. Superconducting magnets, which must be cooled by supercritical helium at temperatures slightly above 4.2 K, are responsible for guiding the beams. The LHC consists of 1104 NbTi superconducting dipole magnets, used to bend the beam around the ring. 128 additional dipole magnets are also used in the beam dump system, which removes the beam from the LHC. Additionally, 392 quadrapole magnets are used to focus the beam in the horizontal and vertical planes. Vacuum chambers ensure that particles do not interact with external residual gas molecules. There are three vacuum systems at the LHC: the insulation vacuum for cryomagnets, the insulation vacuum for helium distribution and the beam vacuum. RF cavities are metallic chambers located inside the beam vacuum. They are designed to resonate at specific frequencies, allowing radio waves to interact with

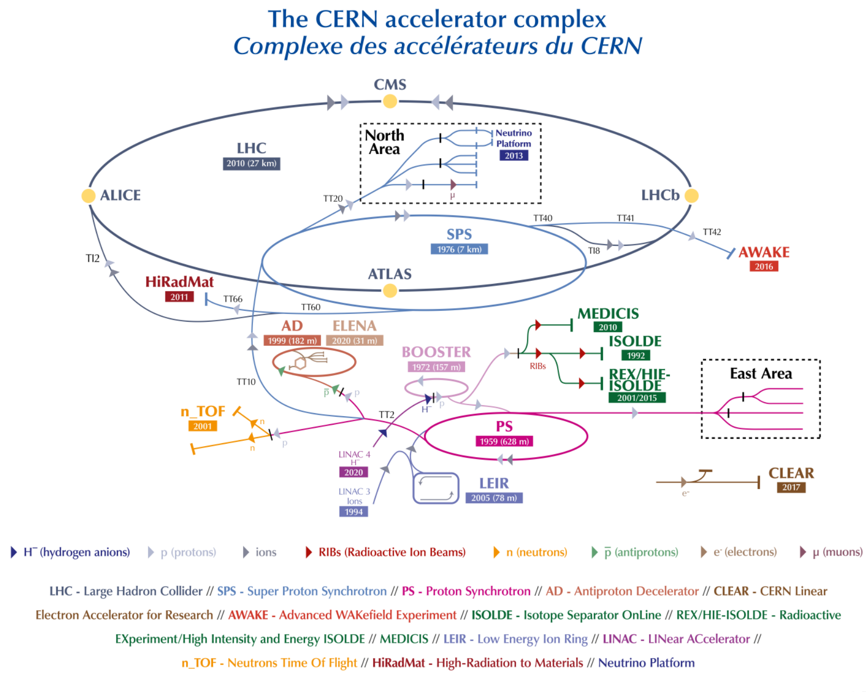

Figure 2.1: The CERN accelerator complex [15].

passing particle bunches. Essentially providing small energy boosts each time the particles pass through.

As of Run 3, the LHC has collided protons at a center of mass energy of $\sqrt{s} = 13.6$ TeV and a peak instantaneous luminosity of $L = 2.1 \times 10^{34} cm^{-2} s^{-1}$, which have surpassed original design. Beams are delivered in bunches with bunch separation of 25 ns, corresponding to a bunch crossing frequency of 40 MHz.

2.2 The ATLAS Apparatus

The ATLAS detector, shown in Figure 2.2, consists of a collection of subsystems confined in a 46m long, 25m in diameter cylinder, 100m below ground. The first subsystem is the Inner Detector (ID), which is responsible for tracking charged-particles. A calorimeter system

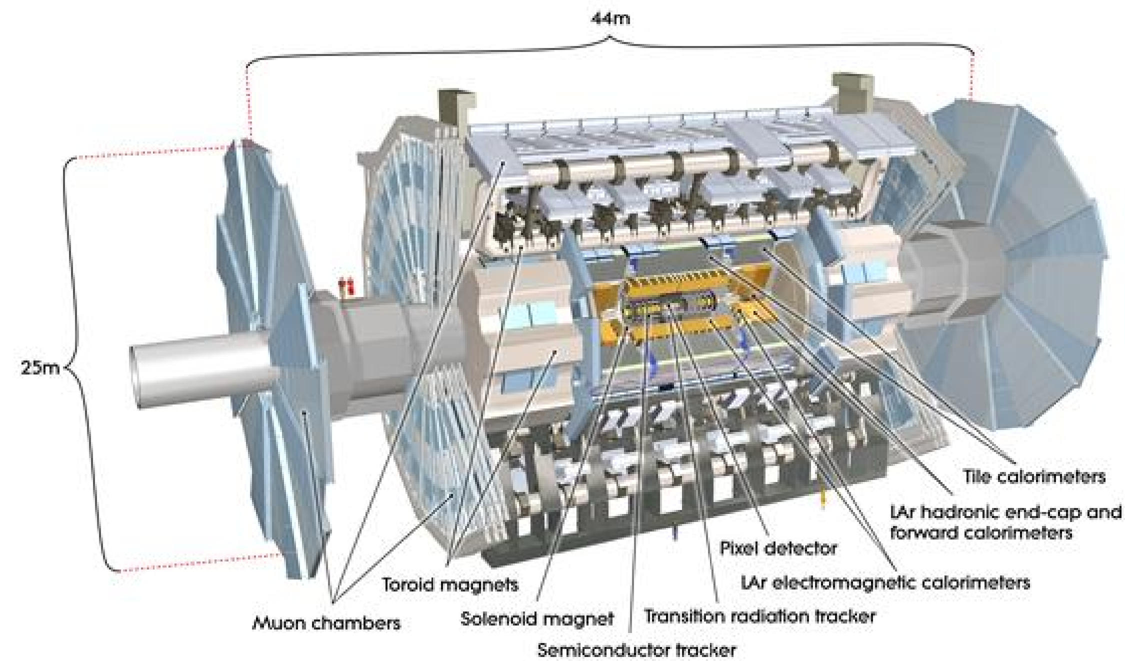

Figure 2.2: Computer generated image of the whole ATLAS detector [16].

follows and measures the energy loss of the particles passing through the detector. The final subsystem is the Muon Spectrometer (MS), which measures the deflection of muons within a magnetic field using a trigger and high precision tracking chambers. Additionally, a first-level and high-level trigger system is implemented to select interesting events and record them to disk.

ATLAS uses a cylindrical coordinate system (r, η, ϕ) for detector design, reconstruction and data analysis. (r, ϕ) are the polar coordinates pointing in the plane towards the center of the LHC ring and upwards. η is the pseudorapidity defined in Equation 2.1, where θ is the polar angle and equal to the true rapidty defined in Equation 2.2.

$$\eta = -\ln(\tan\frac{\theta}{2}) \tag{2.1}$$

$$y = \frac{1}{2}\ln(\frac{E + p_z}{E - p_z}) \tag{2.2}$$

The ID tracks particles in the range $|\eta| < 2.5$, the calorimeter system covers $|\eta| < 4.9$, and the MS detects muon in the $|\eta| < 2.7$ range.

2.2.1 The Inner Detector

The main components of the ID are the Pixel Detector, Semiconductor Tracker (SCT), and the Transition Radiation Tracker (TRT). This layout is provided in Figure 2.3. The Pixel Detector is first to pick up the energy deposits of the collisions at a precision of $10\mu m$. It's coposed of four layers of silicon pixels, over 92 million pixels, providing approximately 80 million readout channels. Their signals determine the origin and momentum of the particles. The SCT surrounds the Pixel Detector and consists of over 4,000 million "micro-strips" of silicon sensors. Their purpose is to measure particle tracks with a precision of up to 25 μm. The TRT is the final layer made up of 300,000 drift tubes interleaved with transition radiation material. These tubes provides information the particle type in combination with the other information gained in the ID.

2.2.2 Calorimeter Systems

Calorimeters are detectors that measure the energies and positions of charged and neutral electromagnetically or strongly interacting particles. They consists of highly-dense materials that force particles to deposit their energy. That energy is then converted into a measurable signal using layers of "active" media. The calorimeter systems consists of two types of calorimeters as shown in Figure 2.4: electromagnetic and hadronic. Electromagnetic calorimeters are used to measure charged particles like electrons, positrons, and photons.

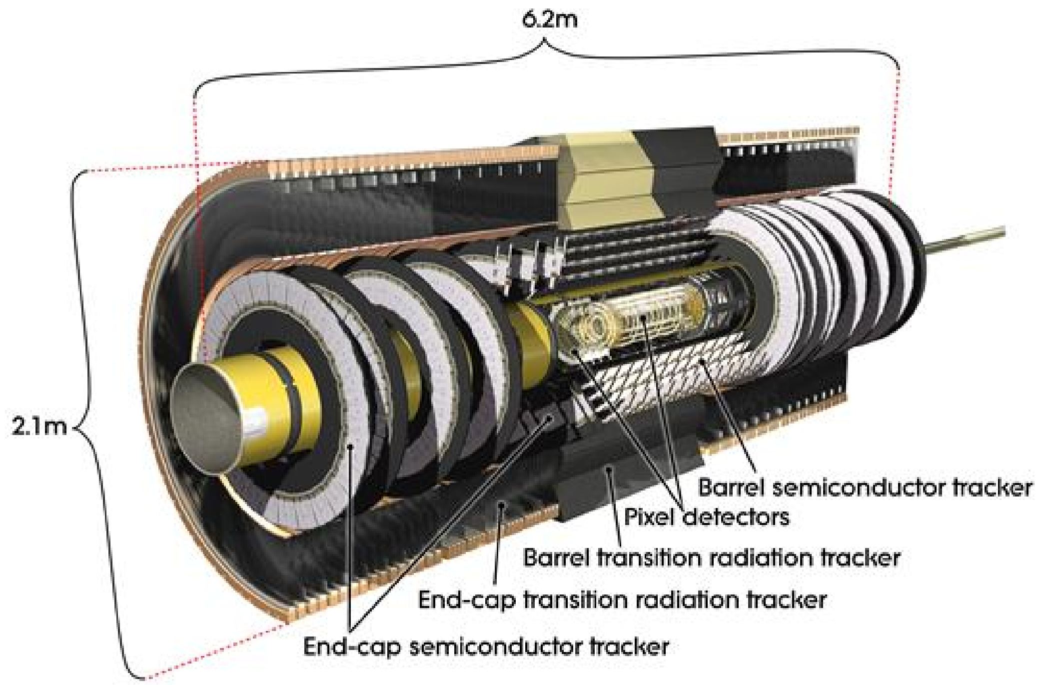

Figure 2.3: Computer generated image of the ATLAS inner detector [17].

Hadronic calorimeters are designed to detect hadrons, such as quarks, protons, and neutrons.

2.2.3 Muon Spectrometer

The muon spectrometer, shown in Figure 2.5, is the outer part of the ATLAS detector, designed to measuring the momentum of muons. Muons are minimally ionizing particles, meaning they can travel to the edge and beyond the ATLAS detector. The magnetic field that bends their directeries is generated by superconducting air-core toroidal magnets, ranging from 2.0 to 6.0 T m across most of the detector. There are also three stations of precision chambers consisting of layers of Monitored Drift Tubes (MDTs). The MDTs are composed of 3 cm wide aluminium tubes filled with a gas mixture, allowing muons to knock out electrongs

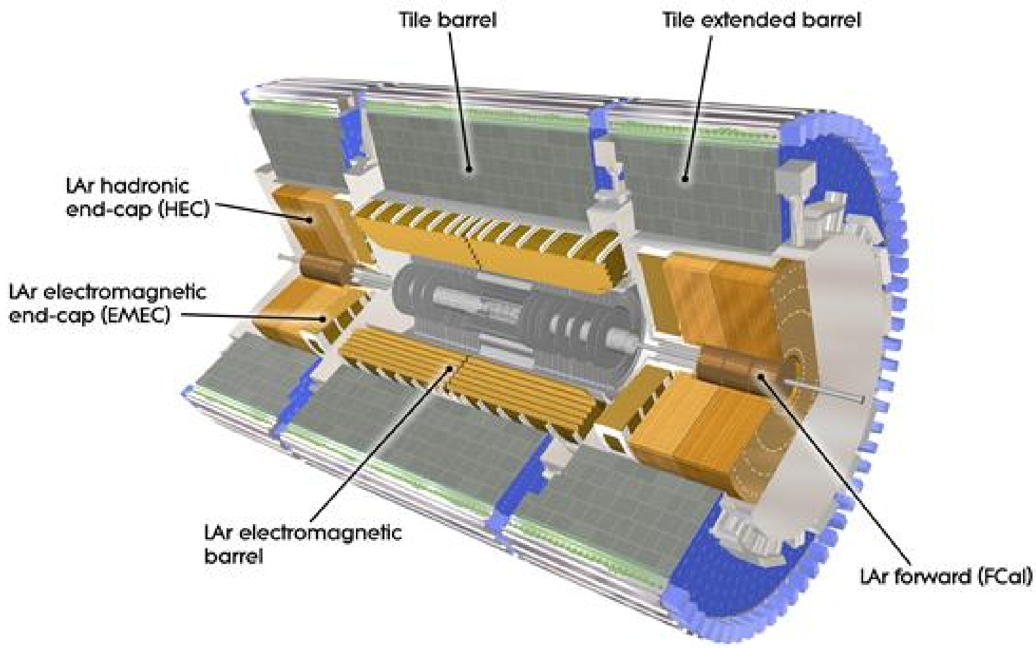

Figure 2.4: Computer generated image of the ATLAS Liquid Argon [18].

from the gas when passing through, to produce a signal. Over 380,000 aluminium tubes are stacked up in several layers over the range of $|\eta| < 2.7$, except in the innermost endcap regions in range $|\eta| > 1.3$. The New Small Wheels (NSW) sit in these endcap regions to detect charged-particle background that get produced as luminosity increases. Two chambers sit sorounding the central region and ends of the experiment: the Resistive Plate Chambers (RPCs) and Thin Gap Chambers (TGCs). RPCs are pairs of parallel plastic plates at an electric potential difference and separated by gas. They sit in the range $|\eta| < 1.0$. TGCs are parallel 50 μm wires in a gas mixture sitting at the ends of the ATLAS experiment in the range $|\eta| > 1.0$. They both detect muons when they ionise the gas mixtures to generate signal.

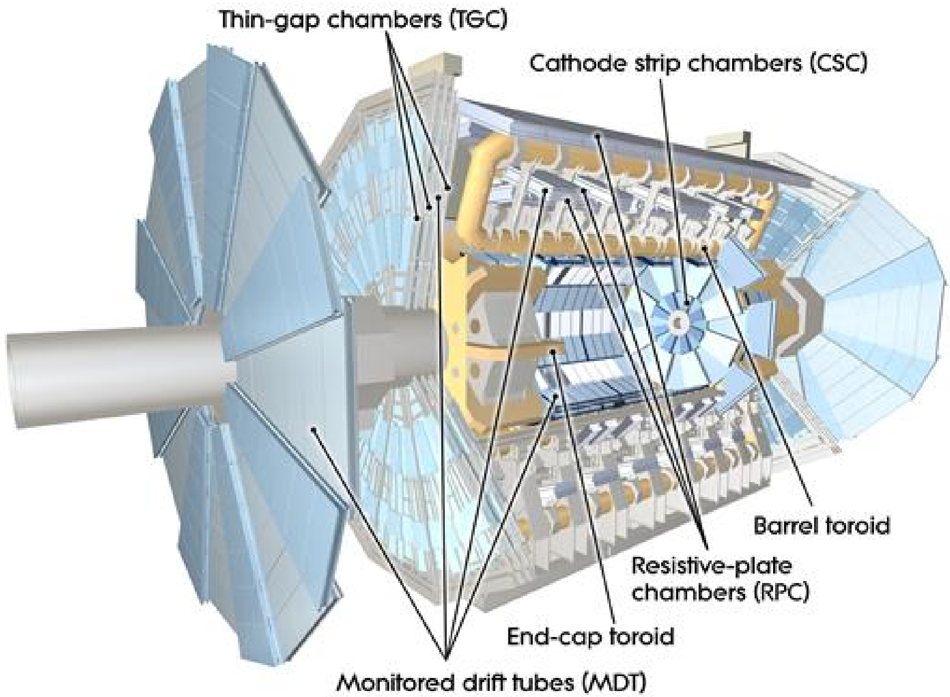

Figure 2.5: Computer generated image of the ATLAS Muons subsystems [19].

2.2.4 Magnet System

The two main magnet systems are the Central Solenoid Magnet and the Toroid Magnets. Generally, superconducting magnets are required to bend the directories of charged particles, allowing for the ATLAS detector to to measure their momentum and charge. The Central Solenoid Magnet provides a 2 Tesla magnetic field surrounding the inner detector. It is 5.8 m long, 2.56 m in diameter and weighs over 5 tonnes. The Toroid Magnets are located at the ends of the experiment, and on massive magnet surrounding the center of the experiment. As mentioned in the previous section, the magnets at the ends of the experiment are to bend muons for the Muon spectrometer.

2.2.5 ATLAS Trigger System

The ATLAS Trigger system is a collection of electronics that make rapid decisions of saving certain events into disk. One full collision event produces about 1.3 MB of data, so reading out at 40 MHz bunch crossing would require a large bandwidth of space. Therefore, there are two trigger subsystems that help selectively read out and store data from interesting physics events. The first level of the trigger system, called the L1 trigger, uses reduced-granularity information from the calorimeters and muon system to search for signatures of these events. The maximum L1 accept rate is 100 kHz, meaning all processing for an event must be completed within that time window. The second level of the trigger system, called L2 trigger, performs a more thorough reconstruction in just 200 μs of the events passed in L1 to then finally pass to a data storage system for offline analysis.

CHAPTER 3

ATLAS SOFTWARE AND COMPUTING

The data collected from the ATLAS data acquisition system must be compared to a set of simulated data. This dataset aims to mimic the different physics processes: it's production by the colliding beams, the evolution of the collision products within the detector and materials, and the detector's response to ultimately interpret efficiencies and background processes. Except for collision data, the output of all these data processing steps are stored in ROOT files. It starts off with Monte Carlo (MC) simulations, which is a computational technique that uses random sampling to generate events. Given these events, the interactions within the detector and the detector's response is simulated. This reconstructed product is called an Analysis Object Data (AOD), which are then cleaned by compressing the data and cutting any unnecessary events or columns into a finalized product called Derived AOD (DAOD). At each step, each produced ROOT file is validated by dedicated tools. These tools collectively encompass the software framework call Athena [31]. The flow of this process is display in Figure 3.1. This chapter will provide an introduction to ROOT and its data storage format called TTree.

3.1 ROOT Introduction

ROOT is a unified software package developed for processing, analyzing, visualizing and ultimately storing the massive high-energy physics datasets into a compressed binary file, called a root file. Previously, high-energy experiments used FORTRAN-based libraries; however, an upgrade was needed to handle the scales and complexities of the data from the

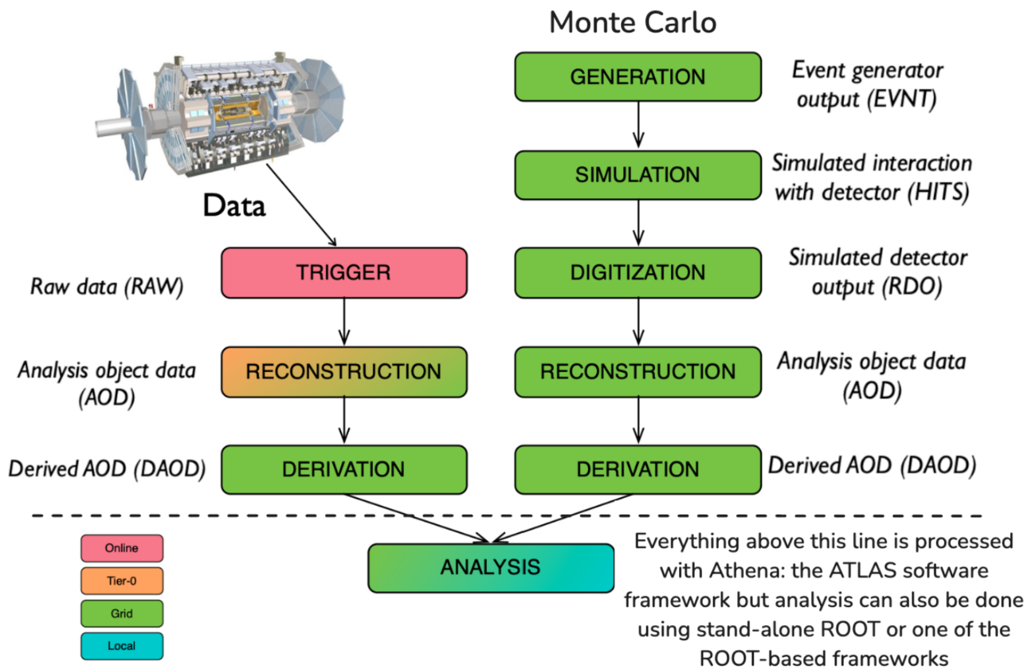

Figure 3.1: ATLAS data chain-processing for data and Monte Carlo simulation [20].

LHC. ROOT maintains an object-oriented structure, meaning it is organized around the data rather than the functions and logic. It's features include visualization tools such as histogramming, and statistical tools. ROOT can be used in C++ and python languages. Several subpackages exists for analysis such as RDataFrame and uproot.

3.1.1 TTree Introduction

ROOT provides a data structure called the TTree to store large amounts of columnar data efficiently. Usually scientific data is stored in what we call row-oriented formats such as a spreadsheet or CSV table. This format is well organized if one wants to access a single event, but viewing a single column then becomes inefficient, especially with large datasets. A TTree is columnar based, meaning it consists of a list of independent columns, called branches. Examples of branches can be event IDs or particle kinematics such as momentum in the x,y,z coordinates. Branches can hold integers, strings and std::vector data types. Buffers are automatically allocated behind each branch. Buffers are temporary storage areas for the independent binary version of the object. This is done to efficiently handle the writing and reading of the data to and from disk. Also, each branch has one or more baskets, which manages the in-memory buffer. In other words, a basket holds the values of a branch for a number of consecutive events. When a buffer is full, it is optionally compressed and then the corresponding basket is written to disk, leading to the creation of a new basket to hold the next entries. ROOT allows users to change buffersize parameters of the branch for personalized optimization. Figure 3.2 shows a more detailed flowchart of the TTree data structure.

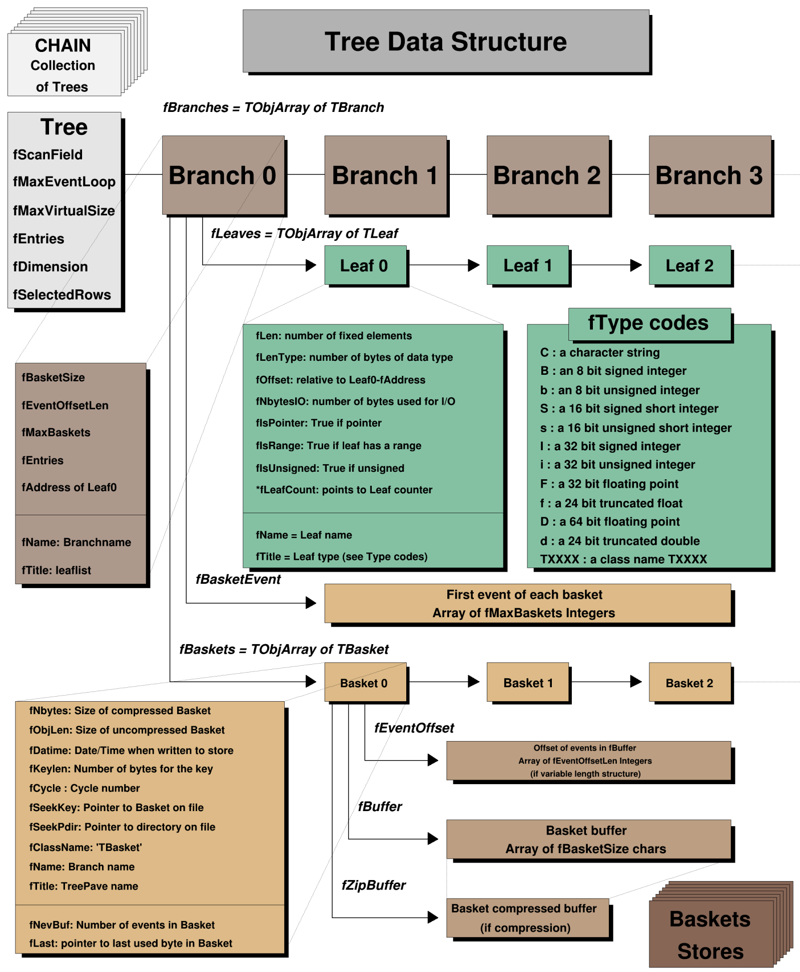

Figure 3.2: Example of the TTree Data Structure [21].

CHAPTER 4

RNTUPLE

RNTuple is the new columnar data format that will be implemented at the start of the HL-LHC. It's design continues to be columnar based, as its predecessor TTree, but it now uses modern storage technologies for better performance charactersitics in data compactness, scalability and read and write speed. For this reason RNTuple classes are backwards-incompatible to TTree both on the file format level and on the API level [23]. It's binary format version follows an *epoch.major.minor.path* scheme, where *epoch* indicates backward-incompatible changes, *major* indicates forward-incompatible changes, *minor* indicates new optional format features, and *patch* indicates backported features from newer format verions. This chapter will introduce the RNTuple structure and user interfaces (UI) for different workflows using the first public release of RNTuple 1.0.0.0.

4.1 Data Structure

RNTuple organizes data using an internal BLOB-based data layout and an external metadata schema. A BLOB (binary large object) is a collection of binary data stored as a single entity. For example, instead of embedding data directly into a database, data can be stored as a BLOB along with a unique identifier for later retreival. This is beneficial for managing large unstructured data [25]. RNTuple uses a similar approach internally: Data is organized by columns of a single type and are attached to *fields*, which describes a serialized C++ type. Columns are partitioned into *pages*. Pages are compressed individually, similar to TTree baskets. *Clusters* are sets of pages that contain all the data belonging to an entry

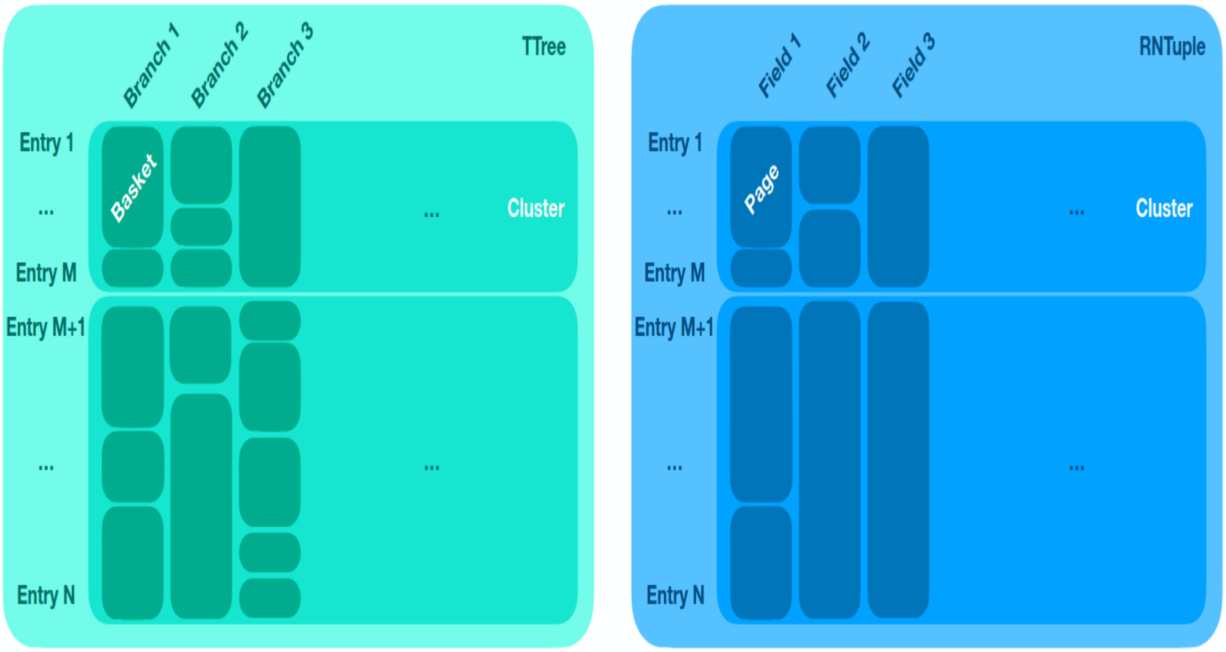

Figure 4.1: TTree Structure vs. RNTuple Structure [22].

range. *Envelopes* are data blocks that contain metadata, such as field and columns types, cluster descriptions, and page locations. Overall, this structure allows for random-access of individual events without decompressing the entire dataset and for "fast merging" or concatenating RNTuples. A simplified diagram of the RNTuple structre in comparison to TTree is shown in Figure 4.1.

4.2 UI

RNTuple API is compatible with RDataFrame analysis workflows and hand-written event loops [24]. The sections below will provide further details and examples.

4.2.1 C++

For hand-written event loops, RNTuple interface uses smart pointers, which simulates a pointer while providing automatic memory management [26]. This feature shortens the amount of code necessary to read and load data by a couple of lines. For example `RNTupleReader::Open` simultaneously loads the ROOT file and the RNTuple. The function `GetView` also simultaneously loads and stores a field. In the example below, the RNTuple is called "EventData" and the field is being stored into the object `electron_pt`, which is the transverse momentum of electrons, "AnalysisElectronsAux:pt".

```
auto ntuple = RNTupleReader::Open("EventData", "DAOD_PHYSLITE.pool.root");
auto electron_pt = ntuple->GetView<std::vector<float>("
    AnalysisElectronsAux:pt");
```

4.2.2 RDataFrame

Analysis done with RDataFrame will mostly remain unmodified with RNTuple, with the exception of filtering. Due to RNTuple's internal data structure, subfields such as "AnalysisElectronsAux:pt" are separated by their field, "AnalysisElectronsAux" by a column, instead of a period. This slight change confuses the filtering function in RDataFrame, but can be bypassed by assigning an alias name:

```
auto df = ROOT::RDF::RNTuple("EventData", "DAOD_PHYSLITE.pool.root");
auto new_df = df.Alias("electron_pt", "AnalysisElectronsAux:pt");
std::string analysis_cut = "(electron_pt.size()>=1&&electron_pt.at(0)
    >25000";
auto filtered_df = new_df.Filter(analysis_cut);
```

CHAPTER 5

RNTUPLE VS. TTREE

In this section, RNTuple performance is analyzed using RDataFrame in C++ and compared to TTree. First, 92 TTrees stored in `DAOD_PHYSLITE` files from ATLAS Open Data [30] were converted to RNTuples using its default compression algorithm setting, ZSTD. Speed tests were performed for loading and outputting RNTuples in comparison to TTrees using `std::chrono::high_resolution_clock::now()`. Each performance study contains two version: a TTree version that uses TTree inputs and an RNTuple version that uses the RNTuple inputs. A comparison of peak memory consumption was also performed using both sets of inputs. This entire process was repeated for RNTuple inputs converted with LZ4 compression algorithm as well.

5.1 Readability Speed

The total loading times for 92 RNTuples and their TTree equivalence were measured 100 times. Loading multiple RNTuples in RDataFrame is the same procedure as done for the TTree version:

```cpp
std::string path = "path_to_files";
std::vector<std::string> filenames;
for (const auto& entry: std::filesystem::directory_iterator(path)){
  std::string filename = entry.path().filename().string();
  filenames.push_back(entry.path().string());
}
auto df = ROOT::RDF::FromRNTuple("EventData", filenames);
```

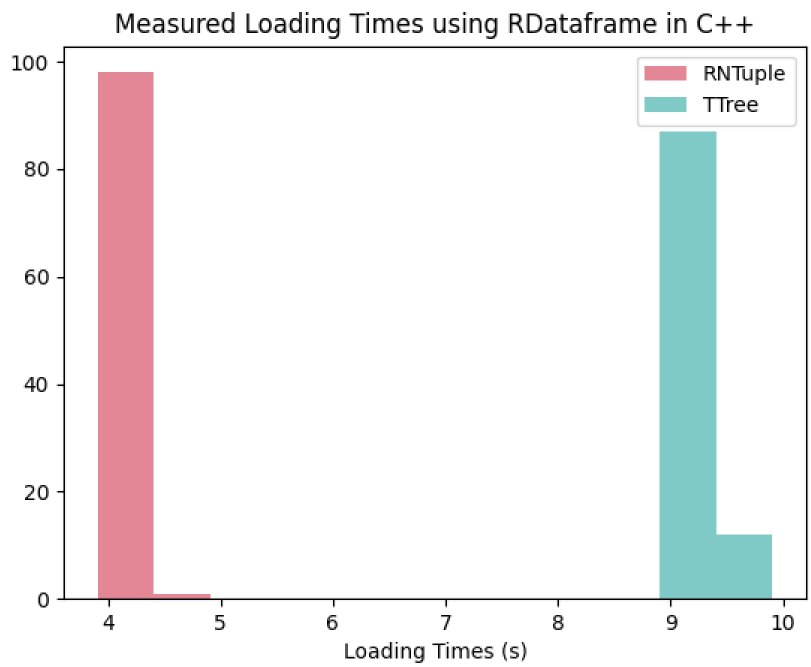

Figure 5.1: Total loading times measured for TTree and RNTuple using RDataFrame in C++.

The timer was stopped after calculating the sum of the column "`AnalysisElectrons:pt`" to ensure that the data was loaded. These times were recorded into a text file and are shown in Figure 5.1. In comparison, this study finds RNTuple to be 2.38 times faster at loading a column of data over TTree.

5.2 Writing Speed

Writing speed was measured by performing an invariant mass calculation and outputting a new data set with two columns: "`ElectronPairsInvMass`" and "`Muon PairsInvMass`". The timer began at the start of an invariant mass calculation and stopped after creating a new dataset. A TTree was written for the TTree version and an RNTuple was written for the RNTuple version. At the start of this study, the lazy function that outputs a TTree in

RDataFrame, `df.Snapshot(...)` was not developed to output an RNTuple; therefore, for consistency, both versions of the script used the RDataFrame function `df.ForEach(...)` to fill in the new columns. This procedure for RNTuple is shown below:

```
auto model = RNTupleModel::Create();
auto e_invm = model->MakeField<ROOT::VecOps::RVec<float>>("ElectronPairsInvMass");
auto m_invm = model->MakeField<ROOT::VecOps::RVec<float>>("MuonPairsInvMass");
auto ntuple = RNTupleWriter::Recreate(std::move(model), "FatisRNTuple", "rnt_invm.root");
df_leptons.Foreach([&](ROOT::VecOps:RVec<float> e_vals, ROOT:VecOps::RVec<float> m_vals){
  *e_invm = e_vals;
  *m_invm = m_vals; ntuple->Fill();
}, {"invm_electrons","invm_muons"});
```

The total output times were recorded in a text file and are shown in Figure 5.2. RNTuple is shown to be 1.51 times faster at writing datasets in RDataFrame C++ than when using TTrees.

5.3 Memory Consumption

The peak memory usage when writing out a dataset was also measured for RNTuple and TTree versions. The same procedure using the invariant mass calculation was repeated 100 times, but using the command `usr/bin/time`. Those measurements are shown in Figure 5.3

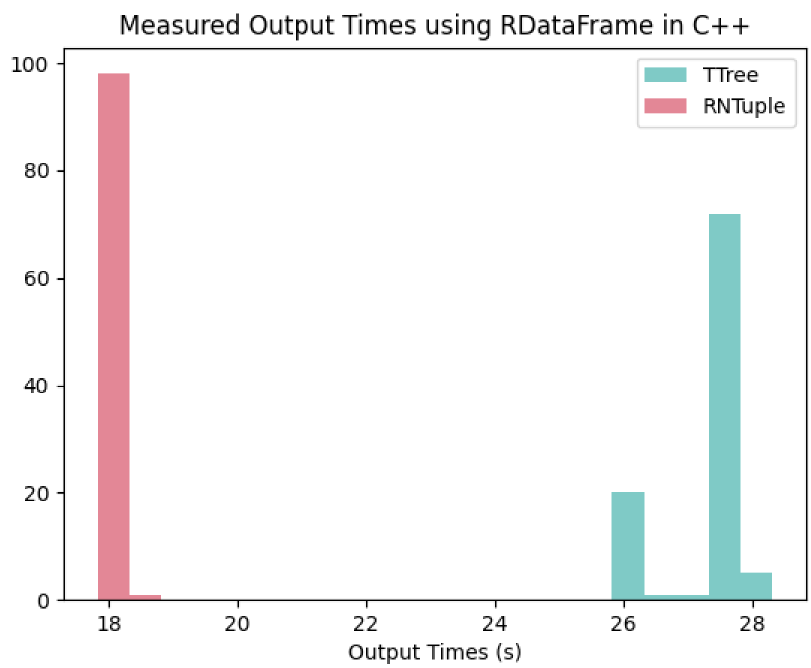

Figure 5.2: Total writing times measured for TTree and RNTuple using RDataFrame in C++.

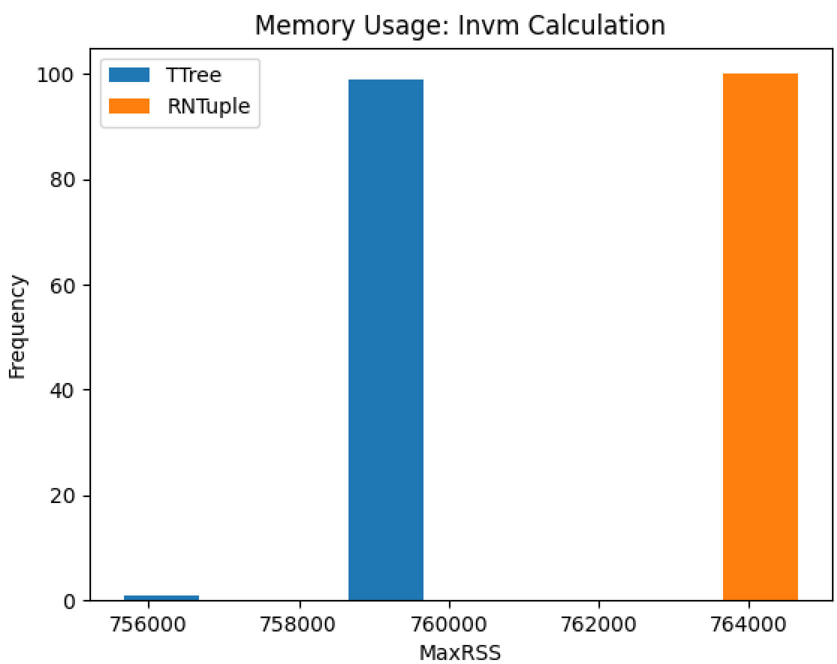

Figure 5.3: Peak memory measurments of TTree and RNTuple writing scripts [NOTE FOR FATIMA: CONSISTENT HISTOGRAM SHADING].

5.4 Compression Algorithms Study

[Under Construction]

CHAPTER 6

ANALYSIS GRAND CHALLENGE: RNTUPLE IMPLEMENTATION

REFERENCES

[1] ATLAS Collaboration. Standard Model summary plots. *ATLAS Public Note ATL-PHYS-PUB-2024-011*, 2024.

[2] ATLAS Collaboration ATLAS: Letter of intent for a general purpose p p experiment at the large hadron collider at CERN. *CERN-LHCC-92-04*, 1992.

[3] ATLAS Collaboration. The ATLAS experiment at the CERN Large Hadron Collider: a description of the detector configuration for Run 3. *JINST*, 19:P05063, 2024. URL: `http://dx.doi.org/10.1088/1748-0221/19/05/P05063`

[4] R. Mann. *An Introduction to Particle Physics and the Standard Model*. Taylor & Francis, 2010. ISBN 978-1-4200-8300-2.

[5] Wikipedia. Elementary particle. URL: `https://en.wikipedia.org/wiki/Elementary_particle`. Accessed: October 9, 2025.

[6] C. N. Yang and R. L. Mills. Conservation of isotopic spin and isotopic gauge invariance. *Phys. Rev.*, 96:191–195, 1954.

[7] P. W. Higgs. Broken symmetries, massless particles and gauge fields. *Phys. Lett.*, 12:132–133, 1964. DOI: 10.1016/0031-9163(64)91136-9.

[8] P. W. Higgs. Broken symmetries and the masses of gauge bosons. *Phys. Rev. Lett.*, 13:508–509, 1964. DOI: 10.1103/PhysRevLett.13.508.

[9] F. Englert and R. Brout. Broken symmetry and the mass of gauge vector mesons. *Phys. Rev. Lett.*, 13:321–323, 1964. DOI: 10.1103/PhysRevLett.13.321.

[10] G. S. Guralnik, C. R. Hagen, and T. W. B. Kibble. Global conservation laws and massless particles. *Phys. Rev. Lett.*, 13:585–587, 1964. DOI: 10.1103/PhysRevLett.13.585.

[11] P. W. Higgs. Spontaneous symmetry breakdown without massless bosons. *Phys. Rev.*, 145:1156–1163, 1966. DOI: 10.1103/PhysRev.145.1156.

[12] ATLAS Collaboration. Observation of a new particle in the search for the Standard Model Higgs boson with the ATLAS detector at the LHC. *Physics Letters B* 716.1 (2012), pp. 1-29

[13] CMS Collaboration Observation of a new boson at a mass of 125 GeV with the CMS experiment at the LHC. *Physics Letters B* 716.1 (Sept. 2012), pp. 30-61

[14] L. Evans and P. Bryant. LHC machine. *JINST*, 3:S08001, 2008.

[15] E. Lopienska. The CERN accelerator complex layout in 2022. Complexe des accelerateurs du CERN en janvier 2022. *CERN-GRAPHICS-2022-001*, 2022. URL: `https://cds.cern.ch/record/2800984`

[16] J. Pequenao Computer generated image of the whole ATLAS detector. *CERN-GE-0803012*, 2008. URL: `https://cds.cern.ch/record/1095924`

[17] J. Pequenao Computer generated image of the ATLAS inner detector. *CERN-GE-0803014*, 2008. URL: `https://cds.cern.ch/record/1095926`

[18] J. Pequenao Computer generated image of the ATLAS Liquid Argon. *CERN-GE-0803016*, 2008. URL: `https://cds.cern.ch/record/1095928`

[19] J. Pequenao Computer generated image of the ATLAS Muons subsystems. *CERN-GE-0803017*, 2008. URL: `https://cds.cern.ch/record/1095929`

[20] J. Catmore The ATLAS data processing chain: from collision to paper. Joint Oslo/Bergen/NBI ATLAS Software Tutorial. University of Oslo, 2016. URL: https://indico.cern.ch/event/472469/contributions/1982677/attachments/1220934/1785823/intro_slides.pdf

[21] ROOT by CERN. TTree Class Reference. *ROOT Reference Guide*. URL: https://root.cern.ch/doc/v630/classTTree.html

[22] A. Serhan Mete,M. Nowak,P. van Gemmeren Persistifying the Complex Event Data Model of the ATLAS Experiment in RNTuple. *22nd International Workshop on Advanced Computing and Analysis Technique in Physics Research*. 11-15 March 2024.

[23] ROOT Team Collaboration RNTuple Binary Format Specification 1.0.0.0 *CERN-OPEN-2025-001* (2024)

[24] J. Blomer,P. Canal,A. Naumann,D. Piparo Evolution of the ROOT TreeIO *EPJ Web of Conf.*245 (2020) 02030

[25] Google Cloud What is binary large object (BLOB) storage? URL: https://cloud.google.com/discover/what-is-binary-large-object-storage

[26] Wikipedia Smart pointer URL: https://en.wikipedia.org/wiki/Smart_pointer

[27] ROOT Team ROOT Reference Documentation URL: https://root.cern.ch/doc/master/index.html

[28] J. Lopez-Gomez, J. Blomer RNTuple performance: Status and Outlook *J. Phys. Conf. Ser.*2438 (2023) 1, 012118

[29] O. S. Bruning, P. Collier,P. Lebrun,S. Myers,R. Ostojic,J. Poole,P. Proudlock LHC Design Report *Geneva:CERN*,2024-548

[30] ATLAS Collaboration URL: https://opendata.atlas.cern/

[31] The ATLAS Collaboration. Athena *Zenodo*, (2019) DOI: https://doi.org/10.5281/zenodo.2641996

[32] J. Blomer,P. Canal,F. de Geus,J. Hahnfeld,A. Naumann,J. Lopez-Gomez,G. Lazzari Miotto,V. E. Padulano ROOT's RNTuple IO Subsystem:The Path to Production *EPJ Web of Conf.*295, 06020 (2024)

APPENDIX

OBJECTIVE SYMPTOMS

Appendices follow the same page-numbering rules as regular chapters. The first page of a multi-page appendix is not numbered. But the page of a single-page appendix *is* numbered.

Are they slow learners or is it a *REAL* problem? These are classic findings in the hopelessly computer challenged.

1. Can't copy from hard drive to disk.
2. Can't eject disks.
3. The word "disk" has thousands of meanings to them. None are correct.
4. Saving a document in any form is a concept totally unexplainable to them.
5. Desktop covered with Untitled Folders - look again, untitled folders are everywhere.
6. "Lost" documents found often in the Apple Menu.
7. Trash always full. Claim they don't know how to place things in trash.
8. Mysterious things happen to their documents or computer when they are not present. AKA "computer victims".
9. Highlighting = deleting. Dragging = Oblivion.
10. Selecting, double-clicking a problem? They will always say their mouse is broken.
11. Their double- click mechanics wants you to send them to a neurologist.
12. Computer always on due to fear of having to restart it.
13. Have never read their QuickMail - will say "I prefer a phone call".
14. Have magical beliefs about what computers do.
15. Describes some flaky way computers could REALLY help them, but is not yet available.

16. Constantly saying they need more “memory”.

17. Requests gizmos and gadgets, i.e., “mouse leash” or “disk cozy”.

18. Avoids eye contact when talking about computers.